Optics and Lasers in Engineering 151 (2022) 106914

Contents lists available at ScienceDirect

Optics and Lasers in Engineering

journal homepage: www.elsevier.com/locate/optlaseng

Calibration method to determine the complete Jones matrix of SLMs

Jesus del Hoyo*, Luis Miguel Sanchez-Brea, Angela Soria-Garcia

Universidad Complutense de Madrid, Applied Optics Complutense Group, Optics Department, Facultad de Ciencias Fisicas, Plaza de las Ciencias, 1, Madrid, 28040 Spain

ARTICLE INFO

Keywords:
Spatial light modulator
Jones matrix
Optical metrology

ABSTRACT

We present a simple method to determine the polarimetric properties of spatial light modulators (SLMs) for each grey level by means of irradiance measurements. The Jones matrix of the SLM is obtained without any assumption about its properties, so it can be applied for more devices than previous works. This method is simple enough to be quickly performed, while offers better results than previous works, as it reduces the error in the prediction of transmission intensities in a factor between 5 and 380.

1. Introduction

Spatial light modulators (SLMs) are a very flexible tool at Optics. Their applications include beam shaping [1–3], holography [4,5], quantum optics [6] and atomic physics [7] among many others. SLMs based on liquid crystal displays (LCDs) and liquid crystal on silicon (LCoS) can spatially manipulate the polarization of light beams. In combination with polarizers and retarders, they can be used to implement amplitude, phase, and even polarization masks. These systems are so flexible that it is possible to change the type of modulation just rotating the polarization elements. However, it is necessary to accurately determine the polarization properties of the SLM (i.e., its Jones matrix for each grey level) to calculate the optimal configuration for each modulation [8].

Several calibration methods have been proposed for determining the Jones matrices of a SLM, which can be divided in two types. The first type models the physical properties of the liquid crystal molecules and how they affect light [9,10]. Then, they can derive the Jones matrices of the SLM with them. The second type of calibration methods ignores the physical properties of the liquid crystal molecules and considers only the optical performance of the system [8,11–18]. It can be used for any SLM, as it does not require prior knowledge about the SLM fabrication materials and techniques. Among them, only the methods described in Refs. [11,12] determine the complete Jones matrices of the SLM. Both methods use interferometric techniques to determine the Jones matrix elements. This requires using a complex setup, very difficult to align. Also, the fringes recorded by the camera must be analyzed using Fourier techniques. The rest of the methods use much simpler setups and calculation techniques. Methods described in Refs. [15–18] directly characterize the amplitude and phase transmission of the SLM, and try to optimize these configurations. Finally, the methods described in Refs. [8,13,14] determine the Jones matrices of the SLM but considering that the SLM behaves as a pure retarder. Therefore, those matrices are not general as they do not consider diattenuation properties the SLM may present.

In this work, we present a new calibration method using a simple setup and simple calculations where no assumptions about the Jones matrix of the SLM are considered. In particular, we drop the assumption that the SLM behaves as a pure retarder. Although this assumption may be a good approximation for some SLMs, we show that SLMs can present diattenuation, so a more general method is required to calibrate them. This method uses a simple setup which requires placing the SLM between several polarizers and retarders and performing several intensity measurements, similar to the methods described in Refs. [8,13,14]. We compare the results obtained using our method with the one developed by Moreno and coworkers [8], since it produces the best results among Refs. [8,13,14] for our SLM. We show that performing just a few more intensity measurements, the errors can be reduced in a factor between 5 and 380 for our model, depending on the configuration of the polarization elements.

2. Calibration method

Polarization properties of a material can be characterized by a 2×2 complex Jones matrix. Therefore, it is completely described by 8 parameters. We chose the description based on the amplitude and phase of the matrix elements

$$J = \exp(i\Phi)\begin{bmatrix} J_0 & J_1 \exp(i\delta_1) \\ J_2 \exp(i\delta_2) & J_3 \exp(i\delta_3) \end{bmatrix}, \quad (1)$$

where the global phase is treated differently as two Jones matrices which only differ in their global phase are equivalent in most cases.

Abbreviations: SLM, Spatial Light Modulator; LCD, Liquid Crystal Display; LCoS, Liquid Crystal on Silicon; PSG, Polarization State Generator; PSA, Polarization State Analyzer.

* Corresponding author.
E-mail address: jhoyo@ucm.es (J. del Hoyo).

https://doi.org/10.1016/j.optlaseng.2021.106914
Received 24 September 2021; Received in revised form 29 November 2021; Accepted 6 December 2021
Available online 23 December 2021

In general, each pixel of the SLM will have a different Jones matrix for each grey level $J_{SLM}(x, y, V)$ and, thus, all 8 parameters will also be different for each pixel and grey level. In order to completely calibrate the Jones matrix, these parameters should be calculated. However, we will not consider inhomogeneities between different pixels, thus only variations between different grey levels will be taken into account.

The calibration of all $J_i(V)$ and $\delta_i(V)$ requires several intensity measurements with a uniform grey level in the SLM. The SLM is placed between a polarization state generator (PSG) and a polarization state analyzer (PSA). A perfect PSG is a system that allows generating any completely polarized state, while a perfect PSA presents maximum transmission for a given totally-polarized state (the analyzed state) and none for its orthogonal state. We will denote the PSG and PSA state using the bra-ket notation [19]. The PSG can be directly represented by its transmitted light state

$$|\phi_G, \chi_G\rangle = \begin{bmatrix} \cos\chi_G \cos\phi_G - i \sin\chi_G \sin\phi_G \\ \cos\chi_G \sin\phi_G + i \sin\chi_G \cos\phi_G \end{bmatrix}, \tag{2}$$

being ϕ_G the state azimuth and χ_G the state ellipticity angle. The case of the PSA is slightly more complex as, in principle, it must be represented by a Jones matrix:

$$J_A = |\phi_A, \chi_A\rangle\langle\phi_A, \chi_A|, \tag{3}$$

where $\langle\phi_A, \chi_A| = |\phi_A, \chi_A\rangle^\dagger$ and † denotes the Hermitian conjugate. Then, the intensity of a Jones vector is calculated as

$$I = |\langle\phi, \chi||\phi, \chi\rangle|^2, \tag{4}$$

so the intensity measured by a detector after the PSA is

$$I_\alpha = \left|\langle\phi_{A\alpha}, \chi_{A\alpha}|J_{SLM}|\phi_{G\alpha}, \chi_{G\alpha}\rangle\right|^2. \tag{5}$$

Then, the configuration of the PSG and PSA for the α intensity measurement is completely determined by four parameters: $\phi_{G\alpha}$, $\chi_{G\alpha}$, $\phi_{A\alpha}$ and $\chi_{A\alpha}$.

2.1. Minimal method

The objective of this type of calibration method is to find a set of configurations for the PSG and PSA which produces a system of equations which can be inverted to determine the parameters of the Jones matrix. The number of possible combinations of PSG and PSA configurations is enormous. In principle, 7 free parameters should be able to be determined by 7 equations, in this case, 7 intensity parameters. However, as we are restricted to intensity measurements, the minimum number of measurements required to completely determine all $J_i(V)$ and δ_i is 10. Even restricted to 10 measurements, there are still a huge number of possible combinations. One of the possibilities is:

$$I_1 = \left|\langle 0°, 0°|J_{SLM}|0°, 0°\rangle\right|^2 = J_0^2, \tag{6a}$$

$$I_2 = \left|\langle 0°, 0°|J_{SLM}|90°, 0°\rangle\right|^2 = J_1^2, \tag{6b}$$

$$I_3 = \left|\langle 90°, 0°|J_{SLM}|0°, 0°\rangle\right|^2 = J_2^2, \tag{6c}$$

$$I_4 = \left|\langle 90°, 0°|J_{SLM}|90°, 0°\rangle\right|^2 = J_3^2, \tag{6d}$$

$$I_5 = \left|\langle 0°, 0°|J_{SLM}|0°, -45°\rangle\right|^2 = \left(J_0^2 + J_1^2 + 2J_0J_1 \sin\delta_1\right)/2, \tag{6e}$$

$$I_6 = \left|\langle 0°, 0°|J_{SLM}|45°, 0°\rangle\right|^2 = \left(J_0^2 + J_1^2 + 2J_0J_1 \cos\delta_1\right)/2, \tag{6f}$$

$$I_7 = \left|\langle 0°, 45°|J_{SLM}|0°, 0°\rangle\right|^2 = \left(J_0^2 + J_2^2 + 2J_0J_2 \sin\delta_2\right)/2, \tag{6g}$$

$$I_8 = \left|\langle 45°, 0°|J_{SLM}|0°, 0°\rangle\right|^2 = \left(J_0^2 + J_2^2 + 2J_0J_2 \cos\delta_2\right)/2, \tag{6h}$$

$$I_9 = \left|\langle 90°, 0°|J_{SLM}|0°, -45°\rangle\right|^2 = \left[J_2^2 + J_3^2 + 2J_2J_3 \sin\left(\delta_3 - \delta_2\right)\right]/2, \tag{6i}$$

$$I_{10} = \left|\langle 90°, 0°|J_{SLM}|45°, 0°\rangle\right|^2 = \left[J_2^2 + J_3^2 + 2J_2J_3 \cos\left(\delta_3 - \delta_2\right)\right]/2, \tag{6j}$$

where the dependence of the grey level has been omitted for clarity. We chose this set of equations for several reasons. First, we implement the PSG and PSA using a rotating polarizer and quarter waveplate. In this way, the required angles for those configurations are multiples of 45°, which is very convenient experimentally. Also, Eqs. (6a)–(6j) are easily invertible. The amplitudes, J_i, are directly obtained from Eqs. (6a)–(6d). The case of phases, δ_i, is slightly more complex, as they always appear inside a sine or cosine function. However, as we have the sine and cosine of each phase, we can use the arc tangent function. The final result is

$$J_0 = \sqrt{I_1}, \tag{7a}$$

$$J_1 = \sqrt{I_2}, \tag{7b}$$

$$J_2 = \sqrt{I_3}, \tag{7c}$$

$$J_3 = \sqrt{I_4}, \tag{7d}$$

$$\delta_1 = \arctan\left(\frac{2I_5 - I_1 - I_2}{2I_6 - I_1 - I_2}\right), \tag{7e}$$

$$\delta_2 = \arctan\left(\frac{2I_7 - I_1 - I_2}{2I_8 - I_1 - I_2}\right), \tag{7f}$$

$$\delta_3 = \arctan\left(\frac{2I_9 - I_3 - I_4}{2I_{10} - I_3 - I_4}\right) + \delta_2, \tag{7g}$$

where arctan considers the sign of the numerator and the denominator to obtain a result between 0° and 360°. We will denote this way of determining the Jones matrix of the SLM as the minimal method.

It is possible to calculate the expected error using the general theory of error propagation:

$$\Delta f(x_1, \ldots, x_N) = \sqrt{\sum_{i=1}^{N} \left(\left|\frac{\partial f}{\partial x_i}\right| \Delta x_i\right)^2}. \tag{8}$$

Considering the error in the intensity measurements is systematic and substituting the value of I_i by the Jones matrix parameters

$$\Delta J_i = \frac{\Delta I}{J_i}, \tag{9a}$$

$$\Delta\delta_1 = \frac{\Delta I}{J_0 J_1}\sqrt{\frac{3}{2} - \frac{1}{2}\sin 2\delta_1}, \tag{9b}$$

$$\Delta\delta_2 = \frac{\Delta I}{J_0 J_2}\sqrt{\frac{3}{2} - \frac{1}{2}\sin 2\delta_2}, \tag{9c}$$

$$\Delta\delta_3 = \sqrt{\left(\frac{\Delta I}{J_2 J_3}\right)^2\left[\frac{3}{2} - \frac{1}{2}\sin 2\left(\delta_3 - \delta_2\right)\right] + \left(\Delta\delta_2\right)^2}. \tag{9d}$$

These equations show that all errors are higher when the involved amplitudes are lower (as $0 \le J_i \le 1$). The errors in the amplitudes only depend on its amplitude themselves, while the error in phases depends on both amplitudes and phases. Also, the errors in the phases are higher for 135° and 315° (when $\sin 2\delta = -1$), and lower for 45° and 135° (when $\sin 2\delta = 1$). The equation $\sqrt{\frac{3}{2} - \frac{1}{2}\sin 2\delta_1}$ is plotted in Fig. 1.

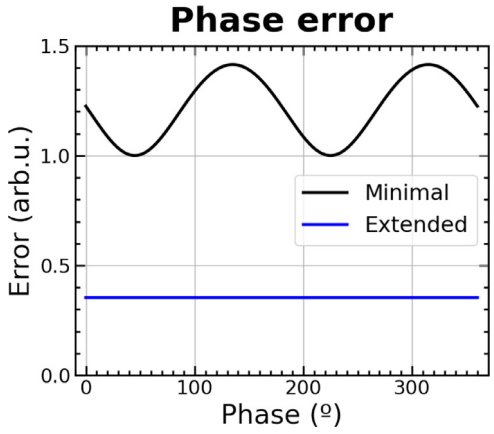

Fig. 1. Expected error of the phases. Error is plotted in arbitrary units as it will depend on the factor $\Delta I/J_i J_j$. In the case of δ_3, the contribution from $\Delta\delta_2$ is neglected.

2.2. Extended method

As we will show in the next section, the minimal method accurately determines J_i. However, the determination of δ_i presents higher errors. For this reason, we developed a new variant of the calibration method in order to reduce that error. It consists of performing 6 additional intensity measurements (16 in total). The configuration of these measurements was chosen maintaining the same criteria used for the minimal method: allowing rotation angles which are multiple of 45° and maintaining an easy way of inverting the equations. The 6 additional selected configurations are

$$I_{11} = \left|\langle 0°, 0°|J_{SLM}|0°, 45°\rangle\right|^2 = \left(J_0^2 + J_1^2 - 2J_0J_1\sin\delta_1\right)/2, \tag{10a}$$

$$I_{12} = \left|\langle 0°, 0°|J_{SLM}|135°, 0°\rangle\right|^2 = \left(J_0^2 + J_1^2 - 2J_0J_1\cos\delta_1\right)/2, \tag{10b}$$

$$I_{13} = \left|\langle 0°, -45°|J_{SLM}|0°, 0°\rangle\right|^2 = \left(J_0^2 + J_2^2 - 2J_0J_2\sin\delta_2\right)/2, \tag{10c}$$

$$I_{14} = \left|\langle 135°, 0°|J_{SLM}|0°, 0°\rangle\right|^2 = \left(J_0^2 + J_2^2 - 2J_0J_2\cos\delta_2\right)/2, \tag{10d}$$

$$I_{15} = \left|\langle 90°, 0°|J_{SLM}|0°, 45°\rangle\right|^2 = \left[J_2^2 + J_3^2 - 2J_2J_3\sin\left(\delta_3 - \delta_2\right)\right]/2, \tag{10e}$$

$$I_{16} = \left|\langle 90°, 0°|J_{SLM}|135°, 0°\rangle\right|^2 = \left[J_2^2 + J_3^2 - 2J_2J_3\cos\left(\delta_3 - \delta_2\right)\right]/2. \tag{10f}$$

Using I_5 to I_{10} measurements from the minimal method and these six new ones, the phases can be calculated as

$$\delta_1' = \arctan\left(\frac{I_5 - I_{11}}{I_6 - I_{12}}\right), \tag{11a}$$

$$\delta_2' = \arctan\left(\frac{I_7 - I_{13}}{I_8 - I_{14}}\right), \tag{11b}$$

$$\delta_3' = \arctan\left(\frac{I_9 - I_{15}}{I_{10} - I_{16}}\right) + \delta_2'. \tag{11c}$$

Again, we can calculate the expected error in the new calculated phases as

$$\Delta\delta_1' = \frac{\Delta I}{\sqrt{8}J_0J_1}, \tag{12a}$$

$$\Delta\delta_2' = \frac{\Delta I}{\sqrt{8}J_0J_2}, \tag{12b}$$

$$\Delta\delta_3' = \frac{\Delta I}{\sqrt{8}J_2}\sqrt{\frac{1}{J_0^2} + \frac{1}{J_3^2}}. \tag{12c}$$

These new errors are a factor between $\sqrt{8}$ and 4 lower than $\Delta\delta_i$, depending on the exact values of the phases.

2.3. Analysis and normalization

There are two methods for testing whether the measured Jones matrices for the SLM correspond to a pure retarder or not. First, pure retarders present the following several mathematical properties [20]:

$$|\det J| = 1, \tag{13a}$$

$$J_0 = J_3, \tag{13b}$$

$$J_1 = J_2. \tag{13c}$$

These condition can be tested after calculating the final Jones matrices. Also, the polar decomposition theorem [20] allows decomposing any Jones matrix in the product of a pure diattenuator (polarizer) and a pure retarder:

$$J_{SLM} = J_D\left(t_{max}, t_{min}, \phi_D, \chi_D\right) J_R\left(\Delta, \phi_R, \chi_R\right). \tag{14}$$

This allows describing the Jones matrices in a different set of components: the maximum and minimum electric field transmissions $t_{\max}$ and $t_{\min}$, the azimuth ϕ_D and ellipticity angle χ_D of the transmission eigenstate of the diattenuator, the retardance Δ and the azimuth ϕ_R and the ellipticity angle χ_R of the fast eigenstate of retarder. Then, it is possible to compare the methods which assumes that the SLM behaves as a pure retarder, as in their case $t_{\max} = t_{\min} = 1$, and ϕ_D and χ_D are not defined.

It is worth noting that Eqs. (6a)–(6j) and Eqs. (10a)–(10f) are not normalized. The methods which model the SLM as a pure retarder [8,13,14] use the same technique for normalization: for each intensity measurement I_i they make an additional measurement $I_i^{\perp}$ using the orthogonal state for the PSA. Then, they normalize the intensity as

$$I_i' = \frac{I_i}{I_i + I_i^{\perp}}. \tag{15}$$

This condition is valid assuming that the SLM behaves as a pure retarder which does not absorb light. However, this is not the case for general Jones matrices, so the intensity must be normalized differently. We choose to normalize to the condition where $\max(t_{\max}) = 1$. Then, any other losses produced by the SLM (for example, due to Fresnel reflections) can be assigned to the system and ignored as they are not polarization dependent.

2.4. Global phase calibration

The global phase Φ must be measured in order to completely determine the Jones matrix of the SLM. It is required in several applications such as implementing phase modulation. Φ can be measured using different methods such as [8,11,17,18]. To do it, we chose an interferometric method, which consists of using a biprism and a camera. The biprism generates a fringes interference pattern. Then, varying the grey level of one half of the pixels of the SLM while maintaining the other one half of the pixels to 0, produces a shift in the fringes. The phase shift can be determined comparing the fringes shift s to their period p,

$$\Phi' = 2\pi\frac{s}{p}. \tag{16}$$

Usually, the measured phase shift has two contributions, the global phase and a contribution derived from the Jones matrix

$$\Phi' = \Phi + \Phi_{Jones}, \tag{17}$$

which depends on the configuration of the PSG and the PSA.

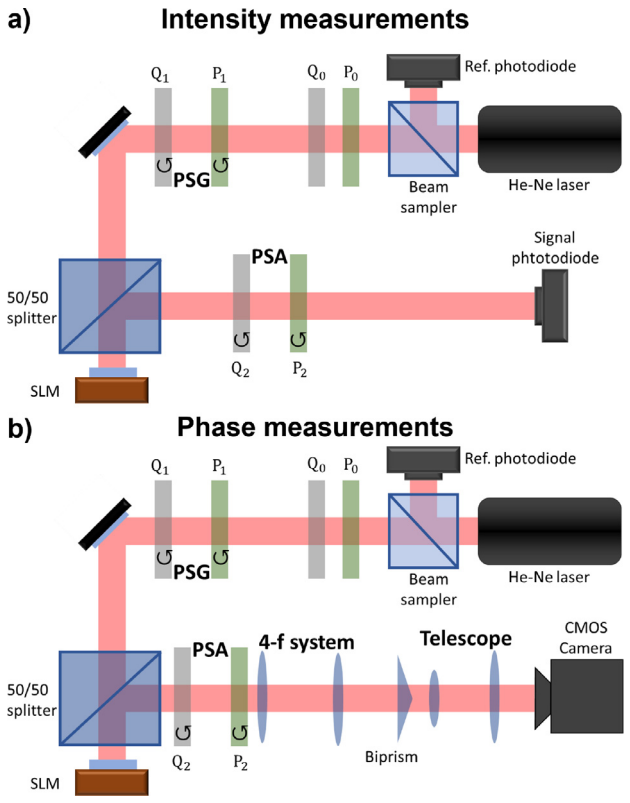

Fig. 2. Schematic representation of the experimental setup in its two different configurations: intensity (a) and phase (b) measurements.

The contribution from the Jones matrix must be subtracted to calculate the real global phase. Fortunately, there is a configuration of the PSG and PSA, $\phi_{PSG} = \chi_{PSG} = \phi_{PSA} = \chi_{PSA} = 0$, where $\Phi_{Jones} = 0$. In that case, the phase shift Φ' is equal to the global phase Φ, avoiding any contribution to the global phase error from the calibration of the rest of the parameters. Nevertheless, it must be checked that the visibility of the fringes is good for all grey levels. If not, a different configuration where the visibility of the fringes does not vary with the grey level should be used, i.e., a near phase modulation configuration.

3. Experimental setup

Fig. 2 shows two schemes of the two configurations of the experimental setup. The illumination consists of a He-Ne laser, with a 633 nm wavelength. We use a beam sampler and a reference photodiode to normalize laser intensity fluctuations. Then, we use a polarizer (P_0) and a quarter waveplate (Q_0) to generate a circularly-polarized light beam. The PSG and PSA are composed by a rotating polarizer ($P_{1,2}$) and a rotating quarter waveplate ($Q_{1,2}$), respectively. We use a non-polarizing 50/50 beam splitter to illuminate the HoloEye LC-R-2500 SLM (resolution 1024x768, 256 levels, 19 μm square pixels) in normal incidence. Finally, we use a second photodiode for the intensity measurements, and a 1° biprism and an Imaging Source DMx 72BUC02 CMOS camera (resolution 2592x1944, 8 bits, 2.2 μm square pixels) for global phase measurements. We have performed an averaging using 25 intensity measurements for each value to reduce experimental errors in the determination of the intensity. During phase measurements, a 4-f system allows relaying the beam at the SLM plane to the biprism plane. Then, a telescope between the biprism and the camera produces a magnification of 7.5 to increase the resolution in the global phase determination. We used *py_pol* open source library [21,22] to perform all required polarization calculations.

4. Results

We performed the calibration of the SLM using the minimal and extended techniques, along with a method which assumes the SLM to behave as a pure retarder for comparison. We chose the method described in Ref. [8] since it is very similar to our method. Also, it is more general than the one described in Ref. [13] and does not require a global minimization method like Ref. [14] which requires significant computational resources (there would be 1024 variables for minimization).

The result is shown in Fig. 3. It has several features worth noting. First, the determined values for J_i using minimal and extended methods are the same, as they are calculated from the same data. Also, both

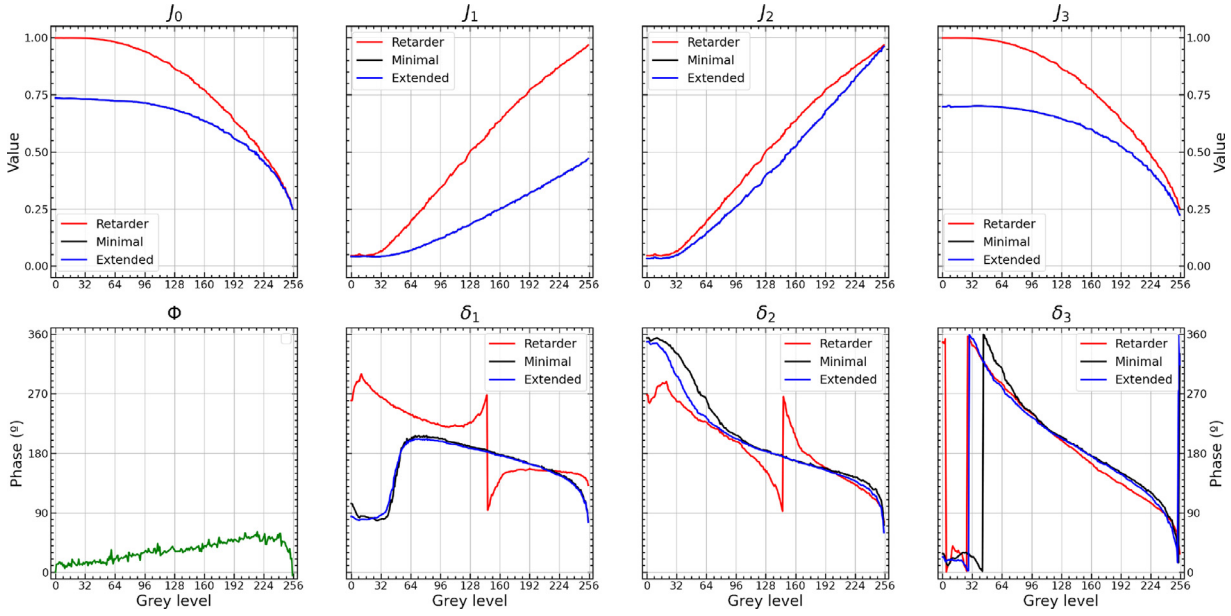

Fig. 3. Calculated Jones matrix elements absolute value (J_i) and phase (δ_i) using a method which assumes the SLM to behave as a pure retarder, and our minimal and extended methods. Results for J_i of minimal and extended methods are equal as they are calculated in the same way. Global phase (Φ) was calculated in the configuration that $\Phi_{Jones} = 0$, so it is independent of the method.

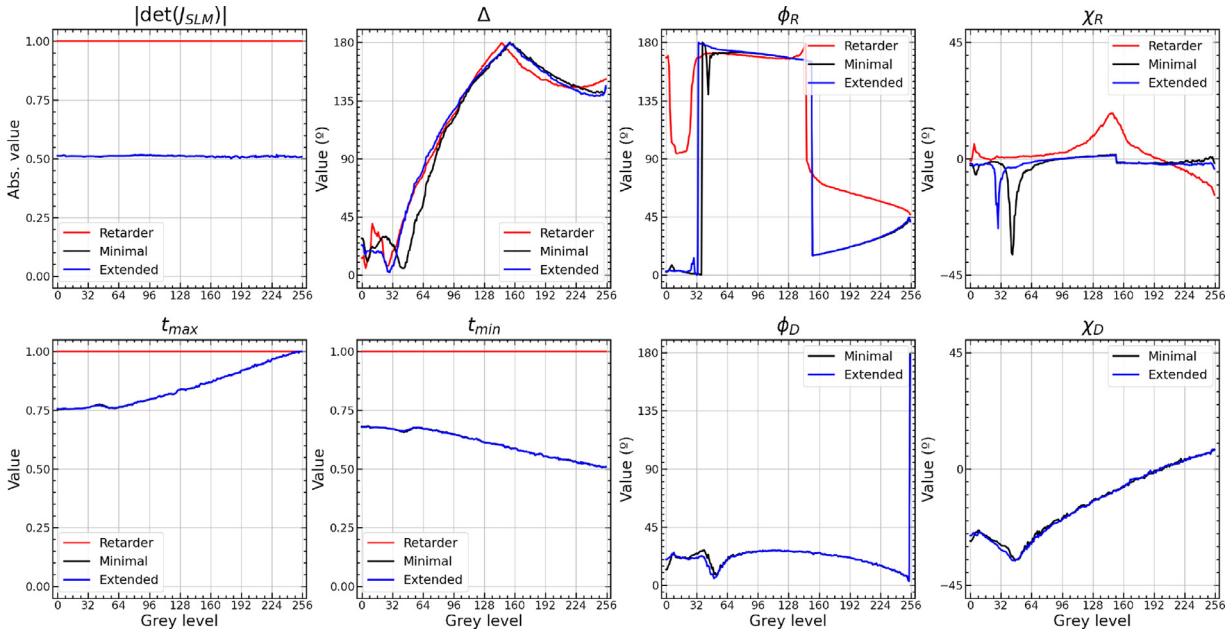

Fig. 4. Calculated absolute value of the determinant of the Jones matrices and the parameters extracted from the decomposition of the Jones matrix in a pure retarder and a pure diattenuator.

methods show minimal differences in δ_1. The differences in δ_2 and δ_3 are slightly greater, the difference in δ_3 caused by the difference in δ_2 (see Eqs. (7g) and (11c)). In addition, it is noticeable that both methods show values incompatible with pure retarder conditions stated in Eqs. (13b) and (13c). Nevertheless, the differences between our methods are much smaller than the differences between any of our methods and the retarder method. J_0, J_1 and J_3 show enormous deviations, while J_2 shows only a moderate deviation.

The differences in δ_1 and δ_2 are also significant. The retarder method shows jumps in phase at grey level 145 around 180° which corresponds to a change of sign in the imaginary phase of those matrix elements. However, the result of δ_3 is very similar, especially compared to the extended method. Interestingly, this tendency can be guessed for δ_1 and specially δ_2, where the phase calculated using the retarder method is somehow similar to the one calculated using the minimal and extended methods except for the lower grey levels (where J_1 and J_2 are small and greater errors in the phase are expected) and near to the phase jumps. Finally, we calculated the global phase using the configuration of $\phi_{PSG} = \chi_{PSG} = \phi_{PSA} = \chi_{PSA} = 0$ so $\Phi_{Jones} = 0$. Its values vary much less than the rest of the phases.

Fig. 4 shows the absolute value of the determinant of the calculated Jones matrices. The mean value of ≈0.51 is really far away from 1, which constitutes a violation of the condition stated in Eq. (13a) for the SLM to be a pure retarder. The difference between minimal and extended method is so small that it cannot be appreciated in the plot (the mean difference is $\approx 3 \times 10^{-4}$).

Fig. 4 also shows the parameters extracted from the decomposition of the Jones matrices in a diattenuator and a retarder. There are little differences in the values obtained for the retardance Δ, specially between the retarder and the extended method. The azimuth of the fast eigenstate ϕ_R presents two jumps. The first one is due to the restriction of this parameter between 0° and 180°. The second one is caused when the retardance goes over 180°, which causes the transformations $\Delta \to 2\pi - \Delta$, $\phi_R \to \pi - \phi_R$ and $\chi_R \to -\chi_R$. The retarder method shows a great difference for low and high grey levels respect to the minimal and extended methods. Finally, we obtained very low ellipticity angles using the three methods (which means that the retarder eigenstates are linear), except some peaks around the $\Delta = 0°$ and $\Delta = 180°$ grey levels, where big errors in this parameter are expected. All this means that, even when the retarder method makes the false assumption that the SLM behaves as a pure retarder, it still correctly predicts the parameters of the retarder part of the Jones matrix.

Table 1
Normalized root mean square errors of the calculations shown in Fig. 5.

Measurement	Normalized RMS error		
	Retarder	Minimal	Extended
I_1	4.7×10^{-2}	3.4×10^{-4}	
I_2	2.0×10^{-2}	9.7×10^{-4}	
I_3	0.38	1.0×10^{-3}	
I_4	6.0×10^{-2}	3.9×10^{-4}	
I_5	7.8×10^{-2}	2.4×10^{-3}	2.1×10^{-3}
I_7	3.6×10^{-2}	3.2×10^{-3}	3.1×10^{-3}
I_9	5.5×10^{-2}	2.0×10^{-3}	1.5×10^{-3}
Independent	4.5×10^{-2}	1.3×10^{-2}	8.7×10^{-3}

There are small differences between the diattenuator parameters calculated using the minimal and extended methods. They show that the difference between maximum and minimum field transmission, $t_{\min}$ and $t_{\max}$, is low for the first grey levels and almost continuously increases until one is the double of the other for the last grey levels. The azimuth of the transmission state ϕ_D remains more or less constant around 22°, and the ellipticity angle χ_D shows that the transmission state is, in general, elliptic.

Finally, Fig. 5 shows the comparison between eight intensity measurements and the calculated intensity using the SLM Jones matrix obtained by the three calibration methods, while Table 1 shows their normalized root mean square (RMS) errors. The first row corresponds to the first four intensity measurements of the minimal and extended calibration methods. The perfect fit of the experimental intensity and the predicted intensity using our method (normalized RMS errors are in the range of $3.4 \times 10^{-4} - 1.0 \times 10^{-3}$) shows that it allows calculating J_i very accurately, in the contrary of the retarder method (normalized RMS errors between 0.02 and 0.4). The first three plots of the second row correspond to the 5th, 7th and 9th intensity measurements which depends on δ_1, δ_2 and $\delta_3 - \delta_2$ respectively (along with J_i). Here the fit is not so perfect (normalized RMS error in the range of $1.5 \times 10^{-3} - 3.1 \times 10^{-3}$), but

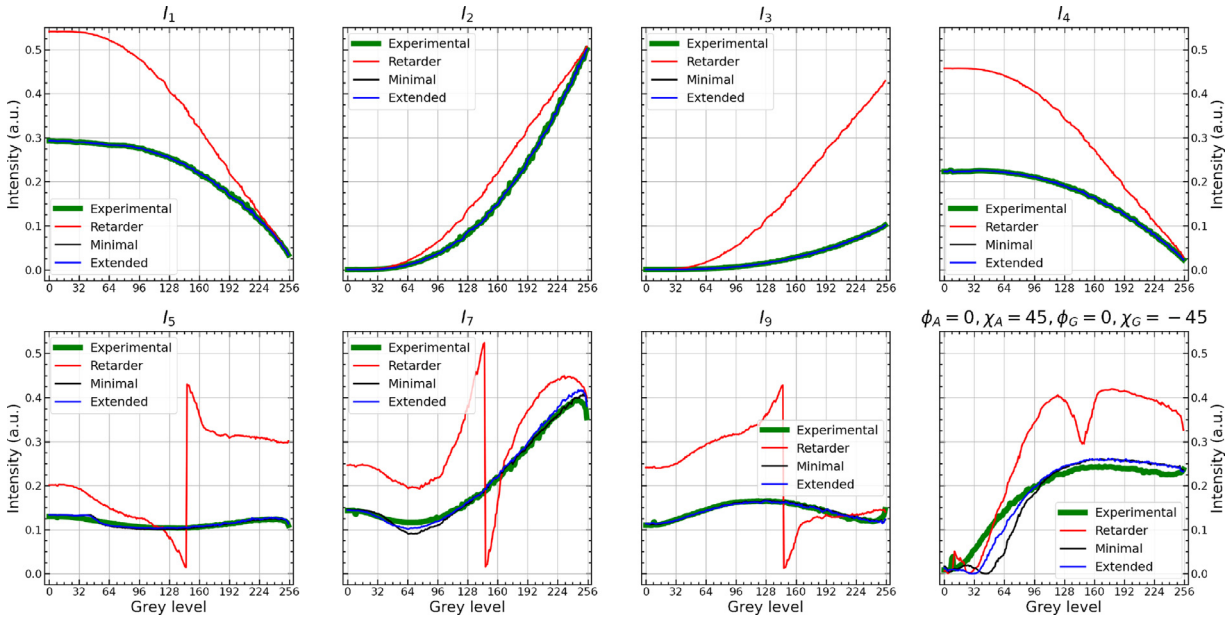

Fig. 5. Experimental and calculated intensities for some configurations of the PSG and PSA.

the deviations are small. This shows that the phases are more sensitive to experimental errors, which inspired the development of the extended method. In all cases, the result obtained using the extended method is better than the one using the minimal method. The ratio is not $\sqrt{8}$, which shows the existence of errors other than systematic. Anyway, the error using the retarder method is still an order of magnitude higher than using our methods. Finally, the last plot of the second row correspond to a measurement which is not included in the 16 measurements of the calibration method. Here, the intensity depends on all parameters of the Jones matrix. Here, minimal and extended methods show more pronounced deviations from experimental values, but still much lower than retarder method.

5. Conclusions

We have developed a simple method for calibrating the complete Jones matrix of SLMs. The method requires performing 10 or 16 intensity measurements for each grey level of the SLM pixels, depending on the precision required. An additional interferometric measurement allows determining the global phase, obtaining the complete Jones matrix. This method does not assume that the SLM behaves as a pure retarder, which allows reducing errors in the prediction of the SLM transmission when the SLM presents diattenuation in a factor between 5 and 380. Finally, this method can be used to characterize the Jones matrix of any optical element, not only SLMs, increasing its utility.

Declaration of Competing Interest

The authors declare that they have no known competing financial interests or personal relationships that could have appeared to influence the work reported in this paper.

CRediT authorship contribution statement

Jesus del Hoyo: Conceptualization, Methodology, Software, Validation, Formal analysis, Investigation, Data curation, Writing – original draft, Writing – review & editing, Visualization, Supervision, Project administration. **Luis Miguel Sanchez-Brea:** Methodology, Software, Resources, Writing – review & editing, Visualization, Supervision, Project administration, Funding acquisition. **Angela Soria-Garcia:** Software, Investigation, Writing – review & editing, Visualization.

Acknowledgements

Authors acknowledge funding from Retos Colaboración 2019 Teluro project RTC2019-007113-3, Ministerio de Economía y Competitivdad and the European Union, European funds for regional development, and from Plan Nacional de Investigación del Ministerio de Ciencia e Innovación Nanorooms project PID2019-105918GB-I00. J. Hoyo acknowledges funding from Programa de Atraccion del Talento from Comunidad de Madrid, 2019-T2/IND-12950.

Supplementary material

Supplementary material associated with this article can be found, in the online version, at doi:10.1016/j.optlaseng.2021.106914.

References

[1] Froehly L, Jacquot M, Lacourt PA, Dudley JM, Courvoisier F. Spatiotemporal structure of femtosecond Bessel beams from spatial light modulators. J Opt Soc Am A 2014;31:790. doi:10.1364/josaa.31.000790.
[2] Siviloglou GA, Christodoulides DN. Accelerating finite energy Airy beams. Opt Lett 2007;32:979. doi:10.1364/ol.32.000979.
[3] Hernandez-Rueda J, Siegel J, Galvan-Sosa M, de la Cruz AR, Garcia-Lechuga M, Solis J. Controlling ablation mechanisms in sapphire by tuning the temporal shape of femtosecond laser pulses. J Opt Soc Am B 2015;32:150. doi:10.1364/josab.32.000150.
[4] Rosen J, Brooker G. Fresnel incoherent correlation holography (FINCH): a review of research. Adv Opt Technol 2012;1:151–69. doi:10.1515/aot-2012-0014.
[5] Tsang PWM, Poon TC. Review on the state-of-the-art technologies for acquisition and display of digital holograms. IEEE Trans Ind Inf 2016;12:886–901. doi:10.1109/TII.2016.2550535.
[6] Zhao L, Guo X, Sun Y, Su Y, Loy MMT, Du S. Shaping the biphoton temporal waveform with spatial light modulation. Phys Rev Lett 2015;115:1–5. doi:10.1103/PhysRevLett.115.193601.
[7] Gaunt AL, Schmidutz TF, Gotlibovych I, Smith RP, Hadzibabic Z. Bose-Einstein condensation of atoms in a uniform potential. Phys Rev Lett 2013;110:1–5. doi:10.1103/PhysRevLett.110.200406.
[8] Moreno I, Velasquez P, Fernandez-Pousa CR, Sanchez-Lopez MM, Mateos F. Jones matrix method for predicting and optimizing the optical modulation properties of a liquid-crystal display. J Appl Phys 2003;94:3697–702. doi:10.1063/1.1601688.
[9] Yamauchi M. Jones-matrix models for twisted-nematic liquid-crystal devices. Appl Opt 2005;44(21):4484–93. doi:10.1364/ao.44.004484.
[10] Marquez A, Campos J, Yzuel MJ, Moreno I, Davis JA, Iemmi CC, et al. Characterization of edge effects in twisted nematic liquid crystal displays. Opt Eng 2000;39:3301–7. doi:10.1117/1.1321197.
[11] Park J, Yu H, Park JH, Park Y. LCD panel characterization by measuring full jones matrix of individual pixels using polarization-sensitive digital holographic microscopy. Opt Express 2014;22:24304. doi:10.1364/oe.22.024304.

[12] Tiwari V, Gautam SK, Naik DN, Singh RK, Bisht NS. Characterization of a spatial light modulator using polarization-sensitive digital holography. Appl Opt 2020;59(7):2024. doi:10.1364/ao.380572.
[13] Ma B, Yao B, Ye T, Lei M. Prediction of optical modulation properties of twisted-nematic liquid-crystal display by improved measurement of Jones matrix. J Appl Phys 2010;107 073107–undefined. doi:10.1063/1.3361238.
[14] Amaya D, Actis D, Rumi G, Lencina A. Least squares method for liquid crystal display characterization. Appl Opt 2017;56:1438. doi:10.1364/ao.56.001438.
[15] Andilla J, Martin-Badosa E, Vallmitjana S. Characterization of a reflective spatial light modulator by determination of its jones matrix, vol. 5622. SPIE; 2004. p. 669–75. doi:10.1117/12.591964.
[16] Khos-Ochir T, Munkhbaatar P, Yang BK, Kim HW, Kim JS, Myung-Whun K. Polarimetric measurement of Jones matrix of a twisted nematic liquid crystal spatial light modulator. J Opt Soc Korea 2012;16:443–8. doi:10.3807/JOSK.2012.16.4.443.
[17] Duran V, Lancis J, Tajahuerce E, Climent V. Poincaré sphere method for optimizing the phase modulation response of a twisted nematic liquid crystal display. IEEE/OSA J Disp Technol 2007;3:9–14. doi:10.1109/JDT.2006.890710.
[18] Ferreira FP, Belsley MS. Direct calibration of a spatial light modulator by lateral shearing interferometry. Opt Express 2010;18:7899. doi:10.1364/oe.18.007899.
[19] Nicolas J, Campos J, Yzuel MJ. Phase and amplitude modulation of elliptic polarization states by nonabsorbing anisotropic elements: application to liquid-crystal devices. J Opt Soc Am A 2002;19:1013.
[20] Gil JJ, Ossikovski R. Polarized light and the Mueller matrix approach, vol 1. CRC press; 2017. ISBN 9781482251562
[21] Hoyo J., Sanchez-Brea L.M.. Py-pol software download at PyPi. 2019a. https://pypi.org/project/py-pol/.
[22] Hoyo J., Sanchez-Brea L.M.. Py-pol documentation at read the docs. 2019b. https://py-pol.readthedocs.io/en/latest/.